Monthly Notices
of the
ROYAL ASTRONOMICAL SOCIETY

MNRAS **488,** L99–L103 (2019)
Advance Access publication 2019 July 04

doi:10.1093/mnrasl/slz106

Exploring a new definition of the green valley and its implications

James Angthopo,[1] Ignacio Ferreras [2,3,4]★ and Joseph Silk [5,6,7]

[1]*Mullard Space Science Laboratory, University College London, Holmbury St Mary, Dorking, Surrey RH5 6NT, UK*
[2]*Department of Physics and Astronomy, University College London, Gower Street, London WC1E 6BT, UK*
[3]*Instituto de Astrofísica de Canarias, Calle Vía Láctea s/n, E-38205 La Laguna, Tenerife, Spain*
[4]*Departamento de Astrofísica, Universidad de La Laguna (ULL), E-38206 La Laguna, Tenerife, Spain*
[5]*Institut d'Astrophysique de Paris (UMR 7095: CNRS & UPMC), 98 bis Bd Arago, F-75014 Paris, France*
[6]*Sub-department of Astrophysics, University of Oxford, Keble Road, Oxford OX1 3RH, UK*
[7]*Department of Physics and Astronomy, The Johns Hopkins University Homewood Campus, Baltimore, MD 21218, USA*

Accepted 2019 June 29. Received 2019 June 28; in original form 2019 February 25

ABSTRACT

The distribution of galaxies on a colour–magnitude diagram reveals a bimodality, featuring a passively evolving red sequence and a star-forming blue cloud. The region between these two, the green valley (GV), represents a fundamental transition where quenching processes operate. We exploit an alternative definition of the GV using the 4000 Å break strength, an indicator that is more resilient than colour to dust attenuation. We compare and contrast our GV definition with the traditional one, based on dust-corrected colour, making use of data from the Sloan Digital Sky Survey. Our GV selection – that does not need a dust correction and thus does not carry the inherent systematics – reveals very similar trends regarding nebular activity (star formation, AGN, quiescence) to the standard dust-corrected ${}^{0.1}(g-r)$. By use of high-SNR stacked spectra of the quiescent GV subsample, we derive the simple stellar population (SSP) age difference across the GV, a rough proxy of the quenching time-scale (Δt). We obtain an increasing trend with velocity dispersion (σ), from $\Delta t \sim 1.5$ Gyr at $\sigma = 100\,\mathrm{km\,s^{-1}}$, up to 3.5 Gyr at $\sigma = 200\,\mathrm{km\,s^{-1}}$, followed by a rapid decrease in the most massive GV galaxies ($\Delta t \sim 1$ Gyr at $\sigma = 250\,\mathrm{km\,s^{-1}}$), suggesting two different modes of quenching, or the presence of an additional channel (rejuvenation).

Key words: galaxies: evolution – galaxies: formation – galaxies: interactions – galaxies: stellar content.

1 INTRODUCTION

Broad-band photometry is widely used to assess the properties of the underlying stellar populations of galaxies. Among the many diagnostic diagrams adopted to study galaxy evolution are the colour–magnitude, or colour–mass, diagram (e.g. Martin et al. 2007, hereafter M07), and the UVJ bi-colour plots (e.g. Whitaker et al. 2011). These diagrams allow us to separate galaxies with respect to the stellar age distribution. However, a colour-based selection requires correcting for dust attenuation, possibly introducing a model-dependent systematic, especially as the attenuation law is found to vary widely among galaxies (e.g. Kriek & Conroy 2013, Narayanan et al. 2018; Tress et al. 2018). An alternative approach would ideally involve the use of age-sensitive indicators that are not so severely affected by dust, suggesting the use of spectral features that could be measured on relatively low-S/N spectra.

The distribution of galaxies on a colour versus magnitude (or versus stellar mass) diagram reveals a conspicuous bimodality (Strateva et al. 2001; Baldry et al. 2004; Bell et al. 2004; Mateus et al. 2006), featuring a Red Sequence (RS), mostly dominated by old and passive galaxies, and a Blue Cloud (BC), made of star-forming (SF) galaxies. The area separating these two populations, termed the green valley (GV), represents a transition region where star formation is quenched (Menci et al. 2005; Faber et al. 2007; Schawinski et al. 2007; Gonçalves et al. 2012; Salim 2014). However, the interpretation of GV galaxies and the process of quenching remains one of the key open questions of galaxy evolution (Schawinski et al. 2014; Taylor et al. 2015; Bremer et al. 2018; Eales et al. 2018).

2 SAMPLE

We make use of a large set of high-quality spectra from the Sloan Digital Sky Survey (SDSS) to define the GV using the standard $D_n(4000)$ feature (Balogh et al. 1999) that quantifies the 4000 Å break strength. This selection is compared with the standard (colour-based) definition of the GV. We select from the

★ E-mail: iferreras@iac.es

SDSS Data Release 14 all individual galaxy spectra (Abolfathi et al. 2018) with a median S/N in the SDSS r band above 10, within the redshift interval $0.05 < z < 0.10$. The original data set comprises 228 880 spectra. We choose the stellar velocity dispersion as the main stacking parameter, instead of the standard choice of either the total luminosity or the stellar mass of the galaxy. The velocity dispersion (σ) is found to correlate more strongly with the underlying population properties (see e.g. Bernardi et al. 2003; Thomas et al. 2005), and is less prone to potential systematics, as it is measured in a straightforward way from the absorption line spectra. The velocity dispersion can be mapped on to stellar mass (M_*) by use of $\log M_*/M_\odot = (1.84 \pm 0.03)\log(\sigma/100\,\mathrm{km\,s^{-1}}) + (10.3 \pm 0.3)$, with the uncertainties quoted at the 68 per cent level. Note also that the velocity dispersion of the spheroidal component correlates well with black hole mass, more strongly than does stellar mass (Gültekin et al. 2009). This will enable us to refine AGN fractions in the GV. The sample is divided into six velocity dispersion bins between $\sigma = 70$ and $250\,\mathrm{km\,s^{-1}}$ in steps of $\Delta\sigma = 30\,\mathrm{km\,s^{-1}}$. We note that with the adopted range of σ, along with the constraint on the S/N of the spectra, the estimates of velocity dispersion provided by the SDSS SpecObj catalogue are reliable.[1]

3 DEFINING THE GREEN VALLEY

We base our definition of the GV on the relative distribution of the SF and quiescent (Q) subsamples. We make use of the MPA-JHU SDSS catalogues (Kauffmann et al. 2003; Brinchmann et al. 2004) that provide a classification of the galaxy spectra from nebular emission lines into SF, AGN, mixed, or quiescent (with the latter class meaning no emission lines are present). We follow a probability-based approach, defining a probability distribution function (PDF) for the BC, $\mathcal{P}_{\rm BC}$, and a PDF for the RS, $\mathcal{P}_{\rm RS}$. These functions are assumed to depend on two parameters only, the stellar velocity dispersion (σ) and an additional parameter (π) that serves as a proxy of the stellar age of the underlying populations. We will compare here two choices, the dust-corrected colour – defined by $(g - r)$ as observed at a fiducial redshift $z = 0.1$ – and the dust uncorrected strength of the 4000 Å break. We adopted the dust correction values from Kauffmann et al. (2003), using the Calzetti et al. (2000) attenuation law, thus enabling a fair comparison to the analysis of M07. Note we use A_V, instead of A_z as baseline for the correction, where we find, at $z = 0.1$, $A_g^{0.1} = 1.16A_V^{0.1}$ and $A_r^{0.1} = 0.88A_V^{0.1}$. For each choice of the second parameter, π, we define the GV as the region where $\mathcal{P}_{\rm BC}(\sigma,\pi) \sim \mathcal{P}_{\rm RS}(\sigma,\pi)$, at fixed velocity dispersion. More specifically, within a velocity dispersion bin, we use the number of observed spectra of SF and quiescent galaxies to define the PDFs of the BC and RS, respectively, fitting them to a Gaussian distribution. The PDF of the GV is then defined as another Gaussian with mean given by the value of π at which $\mathcal{P}_{\rm BC}(\sigma,\pi) = \mathcal{P}_{\rm RS}(\sigma,\pi)$, and standard deviation given by one half of that corresponding to the PDF of the quiescent subsample.

Fig. 1 illustrates the definition of the GV for the choice of $\pi = \mathrm{D}_n(4000)$ (left-hand panels), or $\pi = {}^{0.1}(g - r)$ (dust corrected, right-hand panels), as the population parameter. Both cases show the well-known trend towards higher break strengths or redder colours as velocity dispersion increases. The mean position of the GV is represented by a star symbol. Note the significant difference between the choice of break strength and colour regarding the overlap of the SF and Q subsets. A colour-based approach produces more mixed subsamples that complicates the selection of GV galaxies, whereas the 4000 Å break strength produces a sharper separation.[2] Note, $\mathrm{D}_n(4000)$ provides an alternative, clean separation between BC, GV, and RS *without requiring any dust correction*. Therefore, $\mathrm{D}_n(4000)$ carries a lower systematic uncertainty from the modelling associated with these corrections. This alternative definition of the GV requires low-SNR spectroscopic data, as the 4000 Å break is relatively wide and can be measured even at low spectral resolution (e.g. Hathi et al. 2009; Hernán-Caballero et al. 2013). Our proposed selection of GV galaxies is timely with future spectroscopic surveys on the horizon such as WAVES (Driver et al. 2019), WEAVE (Dalton 2016), DESI (DESI Collaboration 2016), MSE (McConnachie et al. 2016), or J-PAS (Benitez et al. 2014).

Fig. 2 shows the location of the three key evolutionary regions following this methodology, according to $\mathrm{D}_n(4000)$ (left-hand panel), ${}^{0.1}(g - r)$ (uncorrected, centre panel, shown for reference), or ${}^{0.1}(g - r)$ (dust-corrected, right-hand panel). The points with error bars show the mean and standard deviation of each subsample. For reference, individual data points are shown as a density plot. Note the impact on the GV definition between the colour distribution before and after the dust correction is applied. Comparatively, the equivalent dust correction for $\mathrm{D}_n(4000)$ is smaller, resulting in a minor shift of mean in the definition of the RS, BC, and GV subsets, with a maximum $\Delta\mathrm{D}_n(4000) \sim 0.06$ dex. Thus, the 4000 Å break strength produces a clean representation, even without dust correction, of the three phases of evolution under study.

Once the GV is defined, we further separate it into terciles. The lower tercile represents galaxies closer to the BC, and is hereafter defined as the lower green valley (lGV). The upper tercile is closer to the RS and is termed the upper green valley (uGV). If we interpret the GV as a transition region where galaxies quench their star formation, we can portray the lGV and uGV as the starting and ending stages of this transition, respectively.

4 LOOKING INTO THE GREEN VALLEY

Fig. 3 shows the fraction of SF, quiescent and AGN galaxies as a function of velocity dispersion, on the upper and lower GV, contrasting the difference between a selection based on break strength (left), or dust-corrected colour (right). Both methods give the expected decreasing (increasing) trend of SF (quiescent) galaxies towards increasing velocity dispersion, reflecting the effect of downsizing. At the massive end ($\sigma = 200$–$250\,\mathrm{km\,s^{-1}}$), the fraction of AGN in the uGV (lGV) is $\sim 30 \pm 5$ per cent ($\sim 50 \pm 7$ per cent) according to the $\mathrm{D}_n(4000)$ definition, comparable to the equivalent fractions from the dust-corrected colour selection, namely $\sim 37 \pm 6$ per cent ($\sim 51 \pm 8$ per cent). Our estimate of the fractional contribution of AGN is compatible with the analysis of M07 (see Martin et al. 2007, fig. 20), further supporting the idea that the 4000 Å break strength can be accurately used to define the GV without the need for dust correction. Moreover, looking at the distribution of the 4000 Å break strength of M07 in their transition region (see Martin et al. 2007, fig. 3), the index range is fully compatible with our definition of the GV.

If we view the GV as a transition region where galaxies evolve from an SF state into a passive phase, we can compare the stellar

[1] http://classic.sdss.org/dr7/algorithms/veldisp.html

[2] Colours such as $(u - g)$ or $(u - r)$ produce very similar results to $(g - r)$, however we chose the latter as the observations have markedly lower uncertainties.

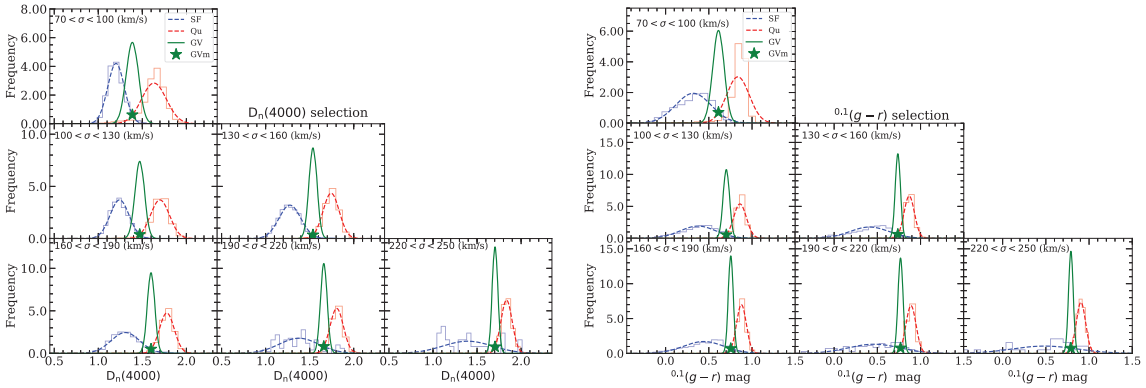

Figure 1. Definition of the GV population: The distribution of star-forming (blue) and quiescent galaxies (red) is used to define a probability distribution function (PDF) for the BC ($\mathcal{P}_{\rm BC}$) and RS ($\mathcal{P}_{\rm RS}$) , respectively. A Gaussian approximation is adopted. The place where $\mathcal{P}_{\rm BC} = \mathcal{P}_{\rm RS}$ defines the mean point of the GV, shown by a star symbol. The green line maps the expected PDF of GV galaxies. The left-hand panels correspond to a selection based on 4000 Å break strength, and the right-hand panels adopt $^{0.1}(g-r)$ colour (dust-corrected) to define the GV.

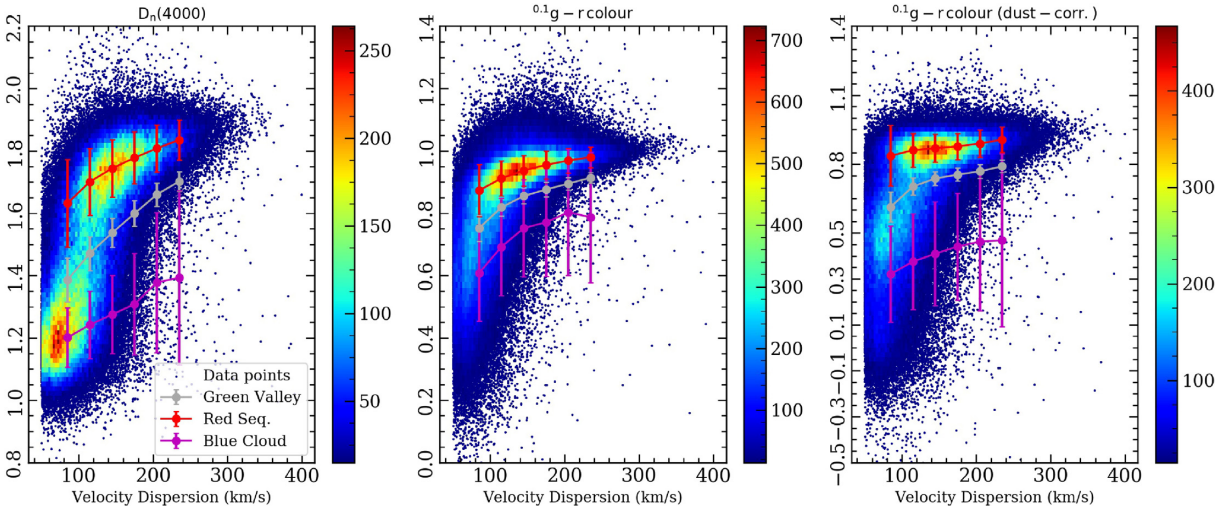

Figure 2. *Left:* Distribution of SDSS galaxies with high-S/N spectra on the D$_n$(4000) versus velocity dispersion plane. The colour map traces number density of individual galaxies on the diagram (colour bar to the right). The BC, GV, and RS subsamples are shown, as labelled, with the points locating the mean of the GV distribution and the error bars spanning the standard deviation (i.e. the corresponding green Gaussians in Fig. 1). *Centre:* Distribution of galaxies on the $^{0.1}(g-r)$ colour (dust-uncorrected, shown for reference) versus velocity dispersion plane. *Right:* Equivalent distribution with the dust-corrected $^{0.1}(g-r)$ colour. Note the D$_n$(4000) measurements have not been corrected for dust, as the correction is negligible for our purposes.

age difference, derived from stellar spectra, to produce an estimate of the time-scale expected to traverse this region. This is a highly non-trivial issue as GV galaxies constitute a motley distribution of systems, and the presence of star formation will bias the estimates of stellar age, as all photospectroscopic indicators are inherently luminosity-weighted, thus heavily biased towards the younger stellar components. The analysis of SF systems typically produce a complex and extended star formation history. Note we have avoided AGN galaxies in the definition and analysis of the GV, as prominent AGN will significantly affect the spectral continuum of the underlying stellar populations, compromising the interpretation of the D$_n$(4000) index as a stellar age-sensitive indicator. Therefore, at the zeroth-order, we focus on the subsample of *quiescent* galaxies in the upper and lower portions of the GV. The difference in stellar age of the quiescent galaxies serves as a proxy of the time galaxies spend on the GV. We now resort to stacking all the quiescent spectra from SDSS, following standard procedures (see e.g. Ferreras et al. 2013). Within a given bin of velocity dispersion, we create one stack in the upper GV and another one in the lower GV. The resulting spectra – mostly featuring S/N above 100 per Å in the regions of interest – are analysed by measuring a set of age- and metallicity-sensitive spectral indices: Hβ, Mgb, and $\langle$Fe$\rangle \equiv$(Fe5270 + Fe5335)/2 (Trager et al. 1998); Hγ_F and Hδ_F (Worthey & Ottaviani 1997); [MgFe]$'$ (Thomas, Maraston & Bender 2003) and the 4000 Å break strength (Balogh et al. 1999). We include a correction for nebular emission in the Balmer lines, following the methodology laid out in appendix B of La Barbera et al. (2013). The observed line strengths are compared with synthetic stellar population models (Vazdekis et al. 2012), producing SSP-equivalent ages (more details will be provided in a follow-up paper to be published in the main journal). The top panels of Fig. 4 show the SSP-equivalent ages of uGV and lGV galaxies with respect to σ, and the bottom panels plot the age difference between these two regions (Δt), that can be interpreted as an

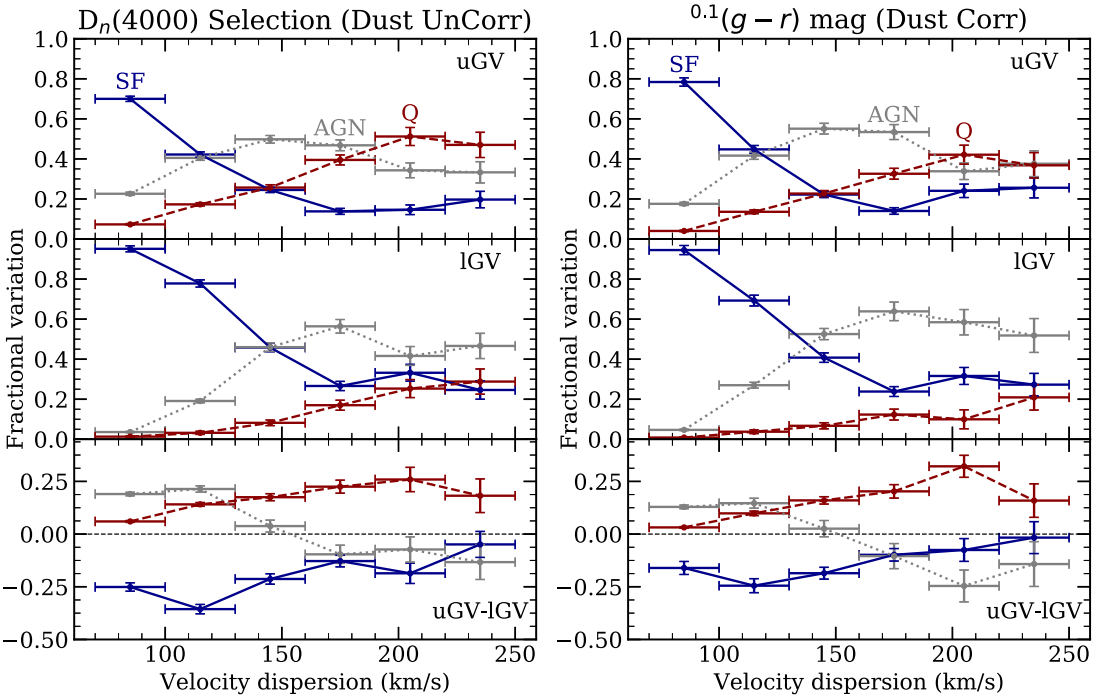

Figure 3. Fraction of galaxy types on the GV. The classification is based on the nebular emission properties, as given by the standard BPT (Baldwin, Phillips & Terlevich 1981) diagram, into SF (blue); AGN/LINER (grey) and quiescent (red). The left-hand (right-hand) panels correspond to the selection of GV galaxies based on 4000 Å strength (dust-corrected colour). From top to bottom, the panels show the fractional contribution according to the spectral type of the upper GV, lower GV, and the difference upper−lower GV.

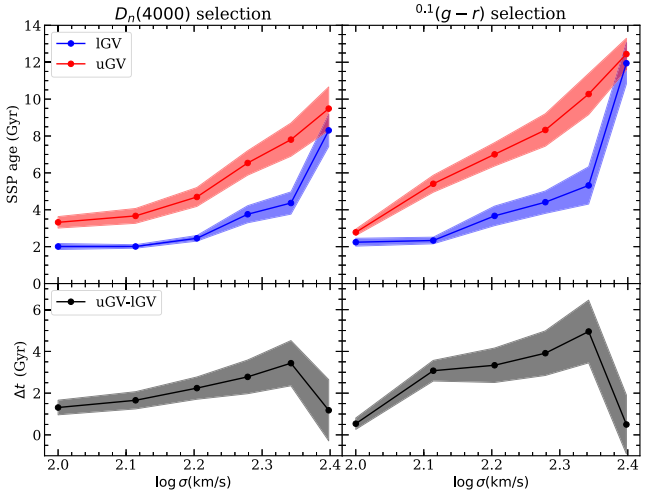

Figure 4. SSP-equivalent age distribution of quiescent galaxies on the GV. The left-hand (right-hand) panels correspond to the selection of the GV based on 4000 Å break strength (dust-corrected colour). The top panels show the ages of upper and lower GV galaxies separately, whereas the bottom panels give the age difference between upper and lower GV at fixed velocity dispersion (defined as Δt). The shaded regions extend over the 1σ uncertainties.

effective quenching time-scale. We emphasize that these differences concern GV galaxies spectroscopically classified as quiescent. The well-known mass–age trend is readily apparent, with more massive galaxies (higher σ) featuring older ages (Gallazzi et al. 2005). It is worth noticing that both the colour and break strength selection produce very similar trends. However at the highest values of velocity dispersion ($\sigma > 190\,\mathrm{km\,s^{-1}}$) the dust-corrected colour selection seems to provide, as absolute SSP ages, older galaxies.

A clearer visualization of this putative GV 'traversing time' can be provided by the difference between SSP ages between the uGV and the lGV. The data feature a trend of increasing Δt with velocity dispersion, implying the GV transit times in more massive galaxies become longer, from $\Delta t \sim 1.5$ Gyr at $\sigma = 100\,\mathrm{km\,s^{-1}}$ to ∼3.5 Gyr at $\sigma = 200\,\mathrm{km\,s^{-1}}$. These values are roughly in line with recent estimates of observed and modelled GV galaxies (Smethurst et al. 2015; Rowlands et al. 2018; Wright et al. 2019), and our analysis suggests a clear trend with respect to velocity dispersion.

Intriguingly, the figure suggests a mass scale – corresponding to the highest velocity dispersion of the stacks – above which the age difference Δt *decreases*, towards GV transition times around 1 Gyr at $\sigma = 250\,\mathrm{km\,s^{-1}}$. These trends can also be found in M07, where a high fraction of AGN with high luminosity is suggestive of short quenching time-scales. In line with M07, we also see a slower quenching regime at lower velocity dispersion ($\sigma < 200\,\mathrm{km\,s^{-1}}$). Such behaviour can be interpreted as two different modes of quenching on either side of this mass scale (if we assume that the transition always proceeds from BC to RS), or the presence of a substantial amount of rejuvenation in higher mass galaxies. Rejuvenation might be due to positive feedback from AGN. This is expected to play a role in early gas-rich phases of massive galaxies, where AGN outflows and precessing jets are likely to overpressurize interstellar gas clouds and induce star formation as in Cen A (Crockett et al. 2012; McKinley et al. 2018; Keel et al. 2019). The simple, clear-cut definition of GV galaxies presented in this letter provides strong constraints on numerical models of galaxy formation (Gabor et al. 2011; Schaye et al. 2015; Dubois et al. 2016; Springel et al. 2018).

ACKNOWLEDGEMENTS

Funding for SDSS-III has been provided by the Alfred P. Sloan Foundation, the Participating Institutions, the National Science Foundation, and the U.S. Department of Energy Office of Science. The SDSS-III website is http://www.sdss3.org. The anonymous referee is thanked for suggestions that substantially improved this letter.

REFERENCES

Abolfathi B. et al., 2018, ApJS, 235, 42
Baldry I. K., Glazebrook K., Brinkmann J., Ivezić Ž., Lupton R. H., Nichol R. C., Szalay A. S., 2004, ApJ, 600, 681
Baldwin J. A., Phillips M. M., Terlevich R., 1981, PASP, 93, 5
Balogh M. L., Morris S. L., Yee H. K. C., Carlberg R. G., Ellingson E., 1999, ApJ, 527, 54
Bell E. F. et al., 2004, ApJ, 608, 752
Benitez N. et al., 2014, preprint (arXiv:1403.5237)
Bernardi M. et al., 2003, AJ, 125, 1882
Bremer M. N. et al., 2018, MNRAS, 476, 12
Brinchmann J., Charlot S., White S. D. M., Tremonti C., Kauffmann G., Heckman T., Brinkmann J., 2004, MNRAS, 351, 1151
Calzetti D., Armus L., Bohlin R. C., Kinney A. L., Koornneef J., Storchi-Bergmann T., 2000, ApJ, 533, 682
Crockett R. M. et al., 2012, MNRAS, 421, 1603
Dalton G., 2016, in Skillen I., Balcells M., Trager S., eds, ASP Conf. Ser. Vol. 507, Multi-Object Spectroscopy in the Next Decade. Astron. Soc. Pac., San Francisco, p. 97
DESI Collaboration, 2016, preprint (arXiv:1611.00036)
Driver S. P. et al., 2019, Messenger, 175, 46
Dubois Y., Peirani S., Pichon C., Devriendt J., Gavazzi R., Welker C., Volonteri M., 2016, MNRAS, 463, 3948
Eales S. A. et al., 2018, MNRAS, 481, 1183
Faber S. M. et al., 2007, ApJ, 665, 265
Ferreras I., La Barbera F., de La Rosa I. G., Vazdekis A., de Carvalho R. R., Falcon-Barroso J., Ricciardelli E., 2013, MNRAS, 429, L15
Gabor J. M., Davé R., Oppenheimer B. D., Finlator K., 2011, MNRAS, 417, 2676
Gallazzi A., Charlot S., Brinchmann J., White S. D. M., Tremonti C. A., 2005, MNRAS, 362, 41
Gonçalves T. S., Martin D. C., Menéndez-Delmestre K., Wyder T. K., Koekemoer A., 2012, ApJ, 759, 67
Gültekin K. et al., 2009, ApJ, 698, 198
Hathi N. P., Ferreras I., Pasquali A., Malhotra S., Rhoads J. E., Pirzkal N., Windhorst R. A., Xu C., 2009, ApJ, 690, 1866
Hernán-Caballero A. et al., 2013, MNRAS, 434, 2136
Kauffmann G. et al., 2003, MNRAS, 341, 33
Keel W. C., Banfield J. K., Medling A. M., Neff S. G., 2019, AJ, 157, 66
Kriek M., Conroy C., 2013, ApJ, 775, L16
La Barbera F., Ferreras I., Vazdekis A., de la Rosa I. G., de Carvalho R. R., Trevisan M., Falcón-Barroso J., Ricciardelli E., 2013, MNRAS, 433, 3017
Martin D. C. et al., 2007, ApJS, 173, 342 M07
Mateus A., Sodré L., Cid Fernandes R., Stasińska G., Schoenell W., Gomes J. M., 2006, MNRAS, 370, 721
McConnachie A. W. et al., 2016, preprint (arXiv:1606.00060)
McKinley B. et al., 2018, MNRAS, 474, 4056
Menci N., Fontana A., Giallongo E., Salimbeni S., 2005, ApJ, 632, 49
Narayanan D., Conroy C., Davé R., Johnson B. D., Popping G., 2018, ApJ, 869, 70
Rowlands K. et al., 2018, MNRAS, 473, 1168
Salim S., 2014, Serb. Astron. J., 189, 1
Schawinski K., Thomas D., Sarzi M., Maraston C., Kaviraj S., Joo S.-J., Yi S. K., Silk J., 2007, MNRAS, 382, 1415
Schawinski K., et al., 2014, MNRAS, 440, 889
Schaye J. et al., 2015, MNRAS, 446, 521
Smethurst R. J. et al., 2015, MNRAS, 450, 435
Springel V. et al., 2018, MNRAS, 475, 676
Strateva I. et al., 2001, AJ, 122, 1861
Taylor E. N. et al., 2015, MNRAS, 446, 2144
Thomas D., Maraston C., Bender R., 2003, MNRAS, 339, 897
Thomas D., Maraston C., Bender R., Mendes de Oliveira C., 2005, ApJ, 621, 673
Trager S. C., Worthey G., Faber S. M., Burstein D., González J. J., 1998, ApJS, 116, 1
Tress M. et al., 2018, MNRAS, 475, 2363
Vazdekis A., Ricciardelli E., Cenarro A. J., Rivero-González J. G., Díaz-García L. A., Falcón-Barroso J., 2012, MNRAS, 424, 157
Whitaker K. E. et al., 2011, ApJ, 735, 86
Worthey G., Ottaviani D. L., 1997, ApJS, 111, 377
Wright R. J., Lagos C. d. P., Davies L. J. M., Power C., Trayford J. W., Wong O. I., 2019, MNRAS, 487, 3740,

This paper has been typeset from a TEX/LATEX file prepared by the author.